Pathological correlates of the magnetization transfer ratio in multiple sclerosis

Marcello Moccia[*1-2], MD, MD(Res), PhD; Steven van de Pavert*[*1], PhD; Arman Eshaghi[1], MD, PhD; Lukas Haider[1], MD, PhD, MBA; Jonas Pichat[3], PhD; Marios Yiannakas[1], PhD; Sebastien Ourselin[3], PhD; Yi Wang[1], MD; Claudia Wheeler-Kingshott[1], PhD; Alan Thompson[1,6], FMedSci; Frederik Barkhof[1,4-6], MD, PhD; and Olga Ciccarelli[1,6], PhD, FRCP.*

*Authors contributed equally.

1. Queen Square MS Centre, NMR Research Unit, Department of Neuroinflammation, UCL Queen Square Institute of Neurology, Faculty of Brain Sciences, University College London, United Kingdom
2. Multiple Sclerosis Clinical Care and Research Centre, Department of Neurosciences, Federico II University, Naples, Italy
3. Centre for Medical Image Computing, Department of Medical Physics and Bioengineering, University College London, United Kingdom
4. Translational Imaging Group, UCL Institute of Healthcare Engineering, University College London, London, United Kingdom
5. Department of Radiology and Nuclear Medicine, VU University Medical Center, Amsterdam, The Netherlands
6. National Institute for Health Research University College London Hospitals Biomedical Research Centre

Authors who completed the statistical analysis: Marcello Moccia, Arman Eshaghi.

CORRESPONDENCE TO: *Olga Ciccarelli*

NMR Research Unit, Queen Square MS Centre, Department of Neuroinflammation

UCL Queen Square Institute of Neurology, Faculty of Brain Sciences

University College London

Russell Square House, 10-12 Russell Square, WC1B5EH London

United Kingdom

Tel: +44 203 108 7415

Fax: +44 207 813 6505

Email: o.ciccarelli@ucl.ac.uk

Word count (Abstract/Text): 250/3518.

Character count (Title): 81.

Number of References/Figures/Tables: 50/4/3.

SEARCH TERMS: multiple sclerosis; MRI; myelin; MTR; magnetization transfer ratio.

DISCLOSURES (relevant to the manuscript)

Marcello Moccia, Steven van de Pavert, Arman Eshaghi, Lukas Haider, Jonas Pichat, Marios Yiannakas, Sebastien Ourselin, Yi Wang, Claudia Wheeler-Kingshott, Alan Thompson, Frederik Barkhof, and Olga Ciccarelli report no disclosures relevant to the manuscript.

FUNDING

The present study received support from the National Institute for Health Research University College London Hospitals Biomedical Research Centre (NIHR UCLH BRC). The authors state that there are no conflicts of interest regarding the publication of this article.

Pathological correlates of the magnetization transfer ratio in multiple sclerosis

ABSTRACT

Objective. To identify pathological correlate(s) of magnetization transfer ratio (MTR) in multiple sclerosis (MS) in a MRI-pathology study.

Methods. We acquired MTR maps at 3T from 16 fixed MS brains and four controls, and immunostained 100 tissue blocks for neuronal neurofilaments, myelin (SMI94), tissue macrophages (CD68), microglia (IBA1), B-lymphocytes, T-lymphocytes, cytotoxic T-lymphocytes, astrocytes (GFAP), and mitochondrial damage (COX4, VDAC). We defined regions-of-interest in lesions, normal-appearing white matter (NAWM) and cortical normal-appearing grey matter (NAGM). Associations between MTR and immunostaining intensities were explored using linear mixed-effects models (with cassettes nested within patients), and interaction terms (for differences between ROIs and between cases and controls); a multivariate linear mixed-effects model identified the best pathological correlate(s) of MTR.

Results. MTR was the lowest in WM lesions (23.4±9.4%), and the highest in NAWM (38.1±8.7%). In MS brains, lower MTR was associated with lower immunostaining intensity for myelin (Coeff=0.31; 95% confidence interval (CI)=0.07,0.55), macrophages (Coeff=0.03; 95%CI=0.01,0.07), and astrocytes (Coeff=0.51; 95%CI=0.02,1.00), and with greater mitochondrial damage (Coeff=0.31; 95%CI=0.07,0.55). Based on interaction terms, MTR was more strongly associated with myelin in WM (Coeff=1.58; 95%CI=1.09,2.08) and GM lesions (Coeff=0.66; 95%CI=0.13,1.20), and with macrophages (Coeff=1.40; 95%CI=0.56,2.25), astrocytes (Coeff=2.66; 95%CI=1.31,4.01), and mitochondrial damage (Coeff=-12.59; 95%CI=-23.16,-2.02) in MS brains than controls. In the

multivariate model, myelin immunostaining intensity was the best correlate of MTR (Coeff=0.31; 95%CI=0.09,0.52; p=0.004).

Conclusions. Myelin was the strongest correlate of MTR, especially in WM and cortical GM lesions, but additional correlates should be kept in mind when designing and interpreting MTR observational and experimental studies in MS.

INTRODUCTION

Defining the pathology specificity of magnetic resonance imaging (MRI) techniques can make them more attractive for experimental clinical trial design, and can help to clarify the underlying mechanisms that are reflected by MRI changes over time.[1] However, *postmortem* MRI-pathological studies are scarce because of the technical challenges posed by the integration of *postmortem* MRI with histologic analysis, the difficulty in obtaining *postmortem* material, the long duration of scanning, and the need for interpretation of normal *postmortem* changes.[2]

Magnetization transfer ratio (MTR) is an objective index of the capacity of macromolecules to exchange magnetization with the surrounding water, indirectly estimating the extent of tissue damage.[3] MTR values are lower in patients with multiple sclerosis (MS) than healthy controls,[4] especially in patients with progressive MS, and with worse motor and cognitive disability.[5] Longitudinal evaluation of MTR changes has been used to reveal the progression of MS pathology *in vivo*,[4,6] and to measure the effectiveness of new medications in experimental clinical trials.[3,7] MTR assessment in these clinical trials has been mostly interpreted as a method to probe myelin status within white matter lesions,[7] although a number of pathology mechanisms are expected to contribute to MTR changes.[8–12] The main pathologic determinant of MTR changes within and outside MS lesions remains unclear.

We aimed to identify the pathology correlate(s) of MTR (primary analysis), and to investigate whether they vary between lesions, normal-appearing (NA) white matter (WM) and cortical grey matter (GM) in MS brains, and between MS and healthy control brains (secondary analyses). We investigated a large sample of MS and healthy control brains, and carried out a comprehensive,

quantitative histology, including a wide range of immunostainings, and employed a novel semi-automatic registration technique.

METHODS

Subjects

Tissue for this study was provided by the United Kingdom MS Tissue Bank at the Imperial College London, under ethical approval from the National Research Ethics Committee. The study followed Human Tissue Act guidelines. All MS patients (n=16) and healthy controls (n=4) had provided informed consent to donate tissue for MS research.

Tissue handling

From each brain, a single coronal cut through mammillary bodies was done to separate brain into anterior and posterior halves. Then, 1 cm-thick coronal slices were cut through entire brain using the 1 cm guide and, for the present study, the second slice posterior to the mammillary bodies towards the occipital pole was included. Slices were immersed in 10% buffered formaldehyde solution for a minimum of seven days, allowing full fixation.

MRI acquisition

The 1 cm-thick coronal slices were used for MRI acquisition. Before scanning, formalin-fixed tissue was washed thoroughly with phosphate-buffered saline (PBS), and placed flat in an MRI-compatible container made of Plexiglas and filled with PBS. The MRI plane was positioned parallel to the coronal tissue slice. Proton density-weighted (PD), T2-weighted (T2) and T1-weighted (T1) spin-echo, and gradient-echo MTR sequences were acquired using a clinical scanner (3T Philips Achieva, Philips Healthcare, Best, Netherlands) with a 32-channel head coil and multi-transmit technology (**Figure 1 a-b**). The MRI acquisition included the whole 1 cm-thick tissue slice. For MTR measurement, two sets of images were obtained using a 3D slab-selective FFE sequence with two echoes (TE1/TE2=5.5/12.7ms), with (M_S) and without (M_0) sinc-Gaussian shaped MT pulses of nominal

α=360°, offset frequency 1 kHz. The two echoes were averaged to increase the signal-to-noise ratio.[13] Then, MTR maps were calculated using the standard equation: $(M_0-M_S/M_0)\times100$. The entire scanning protocol lasted approximately 5 hours and was run at room temperature. Further details on MRI acquisitions are given in the **Table 1**.

Immunohistochemistry

After scanning, brain slices were sectioned into different 5 mm-tick tissue blocks (each approximately 20×30 mm in size) (100 blocks in 20 cases/controls, on average 5.0 blocks per brain slice). Blocks' selection was guided by MRI and visual inspection to improve the sensitivity of the selection process.[14] Serial sections were cut through the block at 5 µm section thickness using the Tissue-Tek AutoSection automated microtome (Sakura Finetek).

Cassettes were paraffin-embedded and immunostained by IQPath (University College London), where immunostain thresholds and reproducibility were preliminary tested (under the supervision of an experienced neuropathologist). Immunostaining was performed using the Ventana Discovery XT instrument and the DAB Map detection Kit (760-124), in compliance with manufacturer instructions. The cassettes were immunostained and quantified for neuronal neurofilaments (NF200; reflecting neuronal density), myelin (myelin basic protein/SMI94; reflecting myelin content) (**Figure 1 c-d**), macrophages (CD68; reflecting tissue macrophages) (**Figure 1 e**), microglia (IBA1), B-lymphocytes (CD20), T-lymphocytes (CD3), cytotoxic T-lymphocytes (CD8), astrocytes (GFAP) (**Figure 1 f**), and mitochondrial activity (COX4, VDAC). Slides were counterstained with haematoxylin (H). Positive and negative controls were included initially when optimizing the stains and, subsequently, only positive controls were included when the antigen was not expected to be present abundantly in the tissue (e.g., CD immunostains).

Immunostained slides were then digitalized as 8-bit RGB images at 40× magnification using a Leica SCN400F slide scanner (Leica Microsystems). Digital image analysis was performed with Definiens Tissue Studio software 3.6 (Definiens AG, Munich, Germany), with a resolution of 5× for tissue identification and a resolution of 10× for stain analysis, taking care to exclude artefacts (e.g., breaks in the section) (**Figure 2**). Images were segmented into pixels of 250×250 μm^2 (0.0625 mm^2). Considering that the degree of staining can vary greatly among tissue blocks, the intensity threshold for positive labelling was set separately for each immunostain, using an automatic histogram method accounting for variation in background stain levels.[15] This histogram method finds the optimal threshold by minimizing the intraclass intensity variance, which simultaneously maximizes interclass variance. Also, the use of nested statistical models further accounted for possible inter-subject variability.

For each pixel, immunostain (brown) intensity and its coordinates were exported in comma-separated values (CSV) files. Details on image processing, quantification and data extraction are reported in **Figure 2**.

Registration

For each cassette, we applied the following three steps to obtain a 2D spatial alignment of MRI and histology:

1) A subject-wise space was created by group-wise registration of digitized histological images, via consecutive rounds of rigid, affine and non-linear registrations with NiftyReg (version 1.3.9);[16,17]

2) The T2-weighted image that best resembled a given histological image with good contrast was chosen. The selected MR plane was cropped to narrow down the search space and, then, rigid

registration was performed. Rigid registration was preferred over non-rigid to preserve the original shape of the tissue without deformation, thereby reducing the possibility of false correspondences between histology and MRI;[17,18]

3) MRI sequences were brought to the group-wise space by applying the inverse transformation from the second step to the selected planes.[16,17]

Image analysis and data extraction

Regions-of-interest (ROIs) were manually delineated on the co-registered MRI and histology with 3D Slicer (version 4.4.0). When MRI-histology co-registration was only partial, ROIs were first delineated on the MRI and then reported to histology. Two assessors (MM and LH) performed the detection of ROIs in agreement, primarily guided by MRI images, with histological images used as references.[19] Lesional and normal-appearing tissues were identified on MRI images, but confirmed on histological images with higher contrast (e.g., SMI94, IBA1, GFAP). ROI area was variable depending on the amount of included tissue. The following ROIs were drawn (number of included ROIs is reported): NAWM (n=100), WM lesions (n=28), cortical NAGM (n=75), and cortical GM lesions (n=33). Overall, 288 records (mean immunostain intensity from different ROIs derived from tissue blocks of cases/controls) were included in the statistical models. To limit the possible impact of artefacts (e.g., coming from superficial dirt on the specimen, tissue scratches, etc.) when using semi-automated approaches, we performed additional manual quality control at two levels: within ROIs (e.g., excluding areas with artefacts from the analysis), and within the quantifications (e.g., going back to the actual staining to check if outliers relate to true genuine histological properties).

Mean MTR signal, mean immunostaining intensity (percentage of stained area) and ROI area were extracted for each ROI using FSL (version 5.0.9). For data analysis, the intensity of mitochondrial

immunostains was combined as follows: percentage of damaged mitochondria = (VDAC-COX4)/VDAC.[20]

Demographic and clinical variables

Demographic and clinical variables were extracted by a neurologist blinded to the pathological analysis, by retrospective review of detailed patients' records. Following variables were collected: age, sex, clinical subtype and disease duration (time from recorded clinical onset to death).

Statistics

At descriptive level, differences in MTR between ROIs in MS brains were measured with linear mixed-effects regression models accounting for the hierarchical structure of data (cassettes nested within patients).

First, to explore the associations between MTR and each stain, we included all the MS regions in linear mixed-effects regression models (mean immunostaining intensity as dependent variable). Fixed-effect variables included in these models were MTR, demographics (age, gender), clinical features (disease duration, clinical subtype), and factors possibly affecting MTR measurement and histology quantification (death-to-fixation interval, ROI type and area). These models used the cassettes as the unit of the analysis, with a random subject intercept to account for the nested structure of the data (cassettes nested within patients). Then, to explore possible variations in the association of MTR and each stain between different ROIs in MS brains, we set an interaction term between ROI (using NAWM as reference) and MTR.

In a second model, we additionally included controls and fitted an interaction term between MTR and disease group to explore possible differences in the association of MTR and each stain between MS brains and controls (controls were used as references). Fixed-effect variables included in these models were MTR, demographics (age, gender), and factors possibly affecting MTR measurement and histology quantification (death-to-fixation interval, ROI area). These models used the cassettes as the unit of the analysis, with a random subject intercept to account for the nested structure of the data (cassettes nested within patients).

Finally, to assess the association between MTR and the mean immunostaining intensities simultaneously, so that the strongest correlate(s) of MTR values could be detected (primary analysis), we fitted a multivariate linear mixed-effects regression model including all immunostaining intensities (assuming an inter-correlation between stains), with a random subject intercept to account for the nested structure of the data (cassettes nested within patients). The multivariate linear mixed-effects regression model was fitted using generalized structural equation modelling. Residuals were checked to confirm model assumptions.

All results are presented as coefficients (Coeff) and 95% confidence intervals (95%CI); p-values are limited to the results of the primary analysis. We used mixed-effects models that shift point estimates and their corresponding intervals toward each other (by a process often referred to as "shrinkage" or "partial pooling"), and, thus, a *post-hoc* correction for multiple comparisons is not necessary.[21]

Stata 15.0 was used for data processing and analysis.

Data availability

Data supporting the findings of this study are available if requested to the authors.

RESULTS

The study included 100 tissue blocks from 16 MS brains (82 tissue blocks) and four healthy controls (18 tissue blocks), from which we derived 288 ROIs. Mean brain weight was 1241.8±151.8 grams. Death-to-fixation interval was 27.1±11.7 hours. Age, gender, death-to-fixation interval, and the number of cassettes are reported in **Table 2**. Both secondary progressive MS (n=11) and primary progressive MS (n=5) brains were studied. Mean disease duration was 27.6±10.5 years.

In MS brains, the lowest MTR was found in the WM lesions (23.4±9.4%), followed by the cortical GM lesions (24.6±7.9%) and cortical NAGM (29.3±7.8%); the NAWM showed the highest MTR values (38.1±8.7%). When comparing the MTR values between MS regions, MTR was lower in WM lesions than NAWM (Coeff=-13.82; 95%CI=-15.61, -12.61), and in cortical GM lesions than cortical NAGM (Coeff=-4.41; 95%CI=-5.69, -3.13); additionally, MTR was lower in cortical NAGM than NAWM (Coeff=-8.59; 95%CI=-9.18, -8.01) (**Figure 3**).

When looking at the associations between MTR and immunostaining intensities in all MS regions at the same time, lower MTR values were associated with lower intensity of immunostaining for myelin (SMI94) (Coeff=0.31; 95%CI=0.07, 0.55) (**Figure 4 a**), macrophages (CD68) (Coeff=0.03; 95%CI=0.01, 0.07) (**Figure 4 b**), and astrocytes (GFAP) (Coeff=0.51; 95%CI=0.02, 1.00) (**Figure 4 c**), and with greater mitochondrial damage (estimated by combining VDAC and COX4) (Coeff=0.31; 95%CI=0.07, 0.55) (**Figure 4 d**). Looking at covariates, disease subtype had no significant effect on the association between MTR and these immunostaining intensities. Coefficients and 95%CI are reported in **Table 3**.

When looking at the differences in the associations of MTR and immunostaining intensities between different regions in MS brains, using NAWM as reference, the association between MTR and myelin content (SMI94) was stronger in WM lesions (Coeff=1.58; 95%CI=1.09, 2.08), and cortical GM lesions (Coeff=0.66; 95%CI=0.13, 1.20), the association between MTR and macrophage density (CD68) (Coeff=0.16; 95%CI=0.09, 0.22) was stronger in WM lesions, the association between MTR and astrocytic density (GFAP) was less strong in cortical GM lesions (Coeff=-1.41; 95%CI=-2.30, -0.52), and the association between MTR and mitochondrial damage (estimated by combining VDAC and COX4) was stronger in cortical NAGM (Coeff=-1.07; 95%CI=-1.83, -0.31). Coefficients and 95%CI are reported in **Table 3**.

When looking at the differences in the associations of MTR and immunostaining intensities between MS brains and healthy controls, the associations between lower MTR and lower densities of macrophages (CD68) (Coeff=1.40; 95%CI=0.56, 2.25), and astrocytes (GFAP) (Coeff=2.66; 95%CI=1.31, 4.01), and greater mitochondrial damage (estimated by combining VDAC and COX4) (Coeff=-12.59; 95%CI=-23.16, -2.02), were stronger in MS brains when compared with healthy controls. Coefficients and 95%CI are reported in **Table 3**.

In the multivariate linear mixed-effects regression model (primary analysis), MTR was associated with myelin content (SMI94) (Coeff=0.31; 95%CI=0.09, 0.52; p=0.004), independently from all the other immunostaining intensities. Coefficients, 95%CI and p-values are reported in **Table 3**.

DISCUSSION

Myelin content, as reflected by the intensity of myelin basic protein immunostaining, was the strongest pathologic correlate of MTR, independently from all other immunostaining intensities. Other pathologic correlates, including macrophages, astrocytes and mitochondrial damage correlated with MTR values more in MS brains, than in the healthy controls. Interestingly, all these associations were not the same between all the MS regions. Before discussing these results in turn, it is useful to highlight the novelties of our study, which are the breadth of immuno-histochemical stains, the inclusion of brains from both MS patients and healthy controls, and the analysis of both lesions and normal-appearing GM and WM. Also, our novel semi-automatic registration technique reduces the risk of false correspondence between different histology and MRI images, and ultimately enables studying antigens which are not expected to be abundant in brain tissue.

When including many different immunostainings in a multivariate linear mixed-effects regression, we found that lower myelin content correlated with lower MTR independently of neuro-axons, lymphocytes, macrophages, astrocytes, and mitochondrial damage, thereby extending and completing the previously reported association between MTR and myelin content.[8,12,22] However, we did not find a significant association between MTR and neuronal immunostaining, suggesting that myelin loss may occur without a concomitant axonal loss, as in the case of chronically demyelinated axons.[23–25] Further studies that include additional pathological techniques (e.g., axonal count, characteristics of residual axons), could help to disentangle the independent contributions of axonal damage and myelin loss to MTR.[3,26]

The relationship between lower MTR and lower myelin content was stronger in both GM and WM lesions, when compared with NAWM, indicating that MTR can be used as a proxy for demyelination

in MS lesions.[2,8,12,22] Demyelination is a common feature of MS pathology and is extensive in WM and GM lesions,[27,28] which showed the lowest MTR values, and less so in NAWM,[29,30] which showed the highest MTR value. By looking at the distribution of myelin immunostaining across the different MS regions, it appears that there was a wider range of values in WM lesions and GM lesions than NAWM, and this could have facilitated the detection of a correlation with MTR. However, the relationship between lower MTR and lower intensity of myelin immunostaining does not necessarily indicate that MTR is a good biomarker of myelin repair; for instance, in active MS, MTR changes also reflect water content (i.e., oedema resolution).[31]

Another reason which should raise attention when interpreting the effect of therapies on MTR values is that other pathological changes occurring in MS are reflected by the MTR values.[31] We found that lower MTR was associated with lower density of macrophages, mainly in the WM lesions. Previous PET imaging studies have reported a heterogeneous pattern of TSPO-BPR28 binding in MS, with WM lesions showing lower TSPO binding, and therefore lower microglial activation, than NAWM,[32] and a higher proportion of inactive lesions in SPMS than relapsing-remitting MS,[32] which agree with our observations. Lower MTR also correlated with lower astrocytic density, mainly in the NAWM. Although the role of astrocytes in MS pathogenesis is not fully understood,[33] it is known that reactive astrocytes acquire a hypertrophic morphology, characterized by massive enlargement of the cell soma and reduced process density.[34] Astroglial hypertrophy is found in MS lesions and adjacent NAWM, and might be caused by oligodendrocyte loss and the resulting disruption of astrocyte–oligodendrocyte networks.[34,35] In any event, the association between MTR and myelin density was significant, independent of the density of astrocytes and macrophages, suggesting MTR is mainly driven by myelin content.

We also found an association between low MTR signal and greater mitochondrial damage, especially in the cortical NAGM. Mitochondrial dysfunction, with subsequent energy failure and oxidative activation, is considered to play an important role in MS pathogenesis.[36,37] Future studies should further explore this association, including specific imaging biomarkers that reflect mitochondrial impairment.[36]

An interesting finding of our study is that the associations between MTR and densities of macrophages and astrocytes, and mitochondrial damage, were stronger in MS brains when compared with healthy controls, suggesting that MS-specific pathology changes can directly affect the MTR signal. As such, an important question would be whether the association between MTR signal and immunostainings is stronger in younger patients with more active disease (e.g., relapsing remitting MS) than in advanced, progressive MS. Unfortunately, we could not address this question in this dataset, since, as expected in *post-mortem* studies, our sample was of rather advanced age and had progressive MS, with a bias towards inactive lesions. However, we have included age, clinical subtype (PPMS or SPMS) and disease duration as covariates in the statistical models to adjust for the possible effects of these variables on our results. Therefore, the extrapolation of our findings to relapsing-remitting MS, which is the population most often studied in clinical trials,[7] should be done with caution.

After death, T1 relaxation time shortens,[38,39] and this can result in lower MTR values.[40] In addition, after formalin fixation, water is removed and its contribution to the MTR signal cannot be analysed.[31] However, in our *post-mortem* sample with fixed brain tissue, MTR values are 5% higher than previous *post-mortem* studies on fixed brain tissue, similar to previous studies on fresh (unfixed) brain tissue,[38,39] and only 5-10% lower than MTR values previously measured *in vivo*.[41]

Also, MTR was significantly different between NAWM and cortical NAGM, and between lesions and their corresponding normal-appearing tissue, as previously described *in vivo* and *ex vivo* (on fixed and unfixed brain tissue).[8,38,39,42] Overall, these findings suggest that we collected good quality data, although we did not assess changes in water content due to tissue fixation.

In this study, we employed the immunostaining intensities rather than the conventional histological metrics (e.g., counts of axons, counts of specific cells, etc.), because we aimed to use a semi-automatic registration technique to align spatially MRI and histology, to reduce inaccuracies in ROI definition, as previously described,[16–18] and performed an intensity-based comparison of a large set of histological markers with MTR. Besides unbiased and reproducible results, the advantages of this approach include: (1) applicability to ROIs, whose shapes limit the application of a strict microscopic counting grid, and (2) possibility to obtain both acellular (myelin) and cellular (T-cells) staining intensities. All histological quantification methods (e.g., numbers of positively stained cells/axons, overall (integrated) staining densities, cut-off level derived measures of area fractions, etc) have specific strengths and drawbacks,[43] and the methodology most suitable to the aim of this project was chosen. The DAB and other immunohistochemical staining techniques, such as "fast blue BB", are not quantitatively enough to support chemical stoichiometry, as the amplification processes are not strictly linear; also, there are multiple other factors that cannot be controlled for, such as slice thickness, temperature, incubation time, pH, etc.[44] However, histological quantification used in this study is well established, and in line with previous literature.[45] Additionally, we used nested statistical models to further account for possible inter-subject variability.

An additional limitation of this study is that we did not apply immunostaining to the whole coronal sections to evaluate the distribution of lesions and inflammation. Further caracterization of neuronal

markers would have been helpful. Image co-registration is challenging for histological sections, inevitably suffering from structural deformations.[46] Cortical lesions are difficult to detect on MRI using MTR sequences, both *in vivo* and on *post-mortem* samples.[47,48] 3T field strenght MRI is known to detect up to 60% of cortical lesions,[49] and is generally considered reliable for cortical lesion detection;[22,49] higher filed strength (e.g., 7T) and smaller slice thickness could further improve cortical lesion detection and classification.[22,48,50] Finally, we could not assess how MTR changes relate to acute inflammation and edema,[31] phenomena that are particularly relevant when MTR is used as a marker of remyelination (e.g., in clinical trials).[3]

In conclusion, myelin immunostaining intensity is the strongest pathology correlate of MTR, especially within lesions. However, MTR values reflect different pathology, such as mitochondrial function, mainly in cortical NAGM, macrophages, mainly in WM lesions, and astrocytes, mainly in NAWM. Therefore, the underlying pathological substrates of MTR values depend on specific brain regions, and this should be kept in mind when interpreting the results of clinical trials which employ MTR as an outcome measure to assess the efficacy of experimental drugs.

ACKNOLEDGEMENTS

Authors thank Prof Sebastian Brandner and Dr Matthew Ellis at the IQPath (UCL Institute of Neurology, University College London) for their support in tissue handling, immunohistochemistry and manuscript preparation.

APPENDIX 1: AUTHORS

Name	Location	Contribution

Marcello Moccia *MD, PhD*	Queen Square MS Centre, NMR Research Unit, Department of Neuroinflammation, UCL Queen Square Institute of Neurology, Faculty of Brain Sciences, University College London, United Kingdom Multiple Sclerosis Clinical Care and Research Centre, Department of Neurosciences, Federico II University, Naples, Italy	Study design; Drafting the manuscript; Analysis of data; Acquisition of data; Statistical analysis.
Steven van de Pavert *PhD*	Queen Square MS Centre, NMR Research Unit, Department of Neuroinflammation, UCL Queen Square Institute of Neurology, Faculty of Brain Sciences, University College London, United Kingdom	Study design; Drafting the manuscript; Analysis of data; Acquisition of data.
Arman Eshaghi *MD, PhD*	Queen Square MS Centre, NMR Research Unit, Department of Neuroinflammation, UCL Queen Square Institute of Neurology, Faculty of Brain Sciences, University College London, United Kingdom	Study design; Drafting the manuscript; Analysis of data; Acquisition of data; Statistical analysis.

Lukas Haider *MD, PhD, MBA*	Queen Square MS Centre, NMR Research Unit, Department of Neuroinflammation, UCL Queen Square Institute of Neurology, Faculty of Brain Sciences, University College London, United Kingdom	Study design; Drafting the manuscript; Analysis of data.
Jonas Pichat *PhD*	Centre for Medical Image Computing, Department of Medical Physics and Bioengineering, University College London, United Kingdom	Study design; Drafting the manuscript; Analysis of data; Acquisition of data.
Marios Yiannakas *PhD*	Queen Square MS Centre, NMR Research Unit, Department of Neuroinflammation, UCL Queen Square Institute of Neurology, Faculty of Brain Sciences, University College London, United Kingdom	Drafting the manuscript; Analysis of data; Acquisition of data.
Sebastien Ourselin *PhD*	Centre for Medical Image Computing, Department of Medical Physics and Bioengineering, University College London, United Kingdom	Study design; Revising the manuscript; Interpretation of data; Study supervision.
Yi Wang *MD, MSc*	Queen Square MS Centre, NMR Research Unit, Department of Neuroinflammation, UCL Queen Square Institute of Neurology, Faculty	Drafting the manuscript; Analysis of data; Acquisition of data.

	of Brain Sciences, University College London, United Kingdom	
Claudia Wheeler-Kingshott PhD	Queen Square MS Centre, NMR Research Unit, Department of Neuroinflammation, UCL Queen Square Institute of Neurology, Faculty of Brain Sciences, University College London, United Kingdom	Study concept; Revising the manuscript; Interpretation of data; Study supervision.
Alan Thompson FMedSci	Queen Square MS Centre, NMR Research Unit, Department of Neuroinflammation, UCL Queen Square Institute of Neurology, Faculty of Brain Sciences, University College London, United Kingdom	Study concept; Revising the manuscript; Interpretation of data; Study supervision.
Frederik Barkhof MD, PhD	Translational Imaging Group, UCL Institute of Healthcare Engineering, University College London, London, United Kingdom Department of Radiology and Nuclear Medicine, VU University Medical Center, Amsterdam, The Netherlands	Study concept; Revising the manuscript; Interpretation of data; Study supervision.
Olga Ciccarelli PhD, FRCP	Queen Square MS Centre, NMR Research Unit, Department of	Study concept; Revising the manuscript;

	Neuroinflammation, UCL Queen Square Institute of Neurology, Faculty of Brain Sciences, University College London, United Kingdom	Interpretation of data; Study coordination.
	National Institute for Health Research University College London Hospitals Biomedical Research Centre	

REFERENCES

1. Wattjes M, Rovira A, Miller D, et al. Evidence-based guidelines: MAGNIMS consensus guidelines on the use of MRI in multiple sclerosis—establishing disease prognosis and monitoring patients. Nat Rev Neurol. 2015;11:597–606.
2. Filippi M, Brück W, Chard D, et al. Association between pathological and MRI findings in multiple sclerosis. Lancet Neurol. 2019;18(2):198–210.
3. Moccia M, de Stefano N, Barkhof F. Imaging outcomes measures for progressive multiple sclerosis trials. Mult Scler. 2017;23(12):1614–1626.
4. Bodini B, Chard D, Altmann DR, et al. White and gray matter damage in primary progressive MS: The chicken or the egg ? Neurology. 2016;86(2):170–176.
5. Stangel M, Kuhlmann T, Matthews PM, Kilpatrick TJ. Achievements and obstacles of remyelinating therapies in multiple sclerosis. Nat Rev Neurol. 2017;13(12):742–754.
6. Chen JT, Collins DL, Atkins HL, et al. Magnetization transfer ratio evolution with demyelination and remyelination in multiple sclerosis lesions. Ann Neurol. 2008;63(2):254–262.
7. Tur C, Moccia M, Barkhof F, et al. Assessing treatment outcomes in multiple sclerosis trials

and in the clinical setting. Nat Rev Neurol. 2018;14(2):75–93.

8. Chen JTH, Easley K, Schneider C, et al. Clinically feasible MTR is sensitive to cortical demyelination in MS. Neurology. 2013;80(3):246–252.

9. Fisher E, Chang A, Fox RJ, et al. Imaging correlates of axonal swelling in chronic multiple sclerosis brains. Ann Neurol. 2007;62(3):219–228.

10. Moll NM, Rietsch AM, Thomas S, et al. Multiple sclerosis normal-appearing white matter: Pathology-imaging correlations. Ann Neurol. 2011;70(5):764–773.

11. Schmierer K, Scaravilli F, Altmann DR, Barker GJ, Miller DH. Magnetization transfer ratio and myelin in postmortem multiple sclerosis brain. Ann Neurol. 2004;56(3):407–415.

12. Schmierer K, Parkes HG, So P-W, et al. High field (9.4 Tesla) magnetic resonance imaging of cortical grey matter lesions in multiple sclerosis. Brain. 2010;133(3):858–867.

13. Pardini M, Sudre CH, Prados F, et al. Relationship of grey and white matter abnormalities with distance from the surface of the brain in multiple sclerosis. J Neurol Neurosurg Psychiatry. 2016;87(11):1212–1217.

14. Bö L, Geurts J, Ravid R, Barkhof F. Magnetic resonance imaging as a tool to examine the neuropathology of multiple sclerosis. Neuropath Appl Neuro. 2004;30(2):106–117.

15. Otsu N. A Threshold Selection Method from Gray-Level Histograms. IEEE Trans Syst Man Cybern. 1979;20(1):62–66.

16. Modat M, Ridgway GR, Taylor ZA, et al. Fast free-form deformation using graphics processing units. Comput Methods Programs Biomed. 2010;98(3):278–284.

17. Pichat J, Iglesias JE, Yousry T, Ourselin S, Modat M. A Survey of Methods for 3D Histology Reconstruction. Med Image Anal. 2018;46:73–105.

18. Lee JS, Ahn S-H, Lee DS, et al. Voxel-based statistical analysis of cerebral glucose metabolism in the rat cortical deafness model by 3D reconstruction of brain from autoradiographic

images. Eur J Nucl Med Mol Imaging. 2005;32(6):696–701.

19. Kilsdonk ID, Jonkman LE, Klaver R, et al. Increased cortical grey matter lesion detection in multiple sclerosis with 7 T MRI: A post-mortem verification study. Brain. 2016;139(5):1472–1481.

20. Shoshan-Barmatz V, De Pinto V, Zweckstetter M, Raviv Z, Keinan N, Arbel N. VDAC, a multi-functional mitochondrial protein regulating cell life and death. Mol Aspects Med. 2010;31(3):227–285.

21. Gelman A, Hill J, Yajima M. Why We (Usually) Don't Have to Worry About Multiple Comparisons. J Res Educ Eff. 2012;5:189–211.

22. Jonkman LE, Fleysher L, Steenwijk MD, et al. Ultra-high field MTR and qR2* differentiates subpial cortical lesions from normal-appearing gray matter in multiple sclerosis. Mult Scler. 2016;22(10):1306–1314.

23. Trapp BD, Vignos M, Dudman J, et al. Cortical neuronal densities and cerebral white matter demyelination in multiple sclerosis: a retrospective study. Lancet Neurol. 2018;17(10):870–884.

24. Haider L, Zrzavy T, Hametner S, et al. The topograpy of demyelination and neurodegeneration in the multiple sclerosis brain. Brain. 2016;139:807–815.

25. DeLuca GC, Williams K, Evangelou N, Ebers GC, Esiri MM. The contribution of demyelination to axonal loss in multiple sclerosis. Brain. 2006;129(6):1507–1516.

26. Grussu F, Schneider T, Tur C, et al. Neurite dispersion: a new marker of multiple sclerosis spinal cord pathology? Ann Clin Transl Neurol. 2017;4(9):663–679.

27. Carassiti D, Altmann DR, Petrova N, Pakkenberg B, Scaravilli F, Schmierer K. Neuronal loss, demyelination and volume change in the multiple sclerosis neocortex. Neuropathol Appl Neurobiol. 2018;44(4):377–390.

28. Prins M, Schul E, Geurts J, van der Valk P, Drukarch B, van Dam AM. Pathological differences between white and grey matter multiple sclerosis lesions. Ann N Y Acad Sci. 2015;1351(1):99–113.

29. Bodini B, Veronese M, García-Lorenzo D, et al. Dynamic imaging of individual remyelination profiles in multiple sclerosis. Ann Neurol. 2016;79(5):726–738.

30. Matías-Guiu JA, Cabrera-Martín MN, Matías-Guiu J, et al. Amyloid PET imaging in multiple sclerosis: an 18F-florbetaben study. BMC Neurol. 2015;15(1):243.

31. Vavasour IM, Laule C, Li DKB, Traboulsee AL, MacKay AL. Is the magnetization transfer ratio a marker for myelin in multiple sclerosis? J Magn Reson Imaging. 2011;33(3):713–718.

32. Datta G, Colasanti A, Kalk N, et al. 11C-PBR28 and 18F-PBR111 detect white matter inflammatory heterogeneity in multiple sclerosis. J Nucl Med. 2017;58(9):1477–1482.

33. Ponath G, Park C, Pitt D. The Role of Astrocytes in Multiple Sclerosis. Front Immunol. 2018;9:217.

34. Brosnan CF, Raine CS. The astrocyte in multiple sclerosis revisited. Glia. 2013;61(4):453–465.

35. Orthmann-Murphy JL, Abrams CK, Scherer SS. Gap Junctions Couple Astrocytes and Oligodendrocytes. J Mol Neurosci. 2009;35(1):101–116.

36. van Horssen J, Witte M, Ciccarelli O. The role of mitochondria in axonal degeneration and tissue repair in MS. Mult Scler. 2012;18(8):1058–1067.

37. Haider L, Fischer MT, Frischer JM, et al. Oxidative damage in multiple sclerosis lesions. Brain. 2011;134:1914–1924.

38. Schmierer K, Wheeler-Kingshott CAM, Tozer DJ, et al. Quantitative magnetic resonance of postmortem multiple sclerosis brain before and after fixation. Magn Reson Med. 2008;59(2):268–277.

39. Schmierer K, Thavarajah JR, An SF, Brandner S, Miller DH, Tozer DJ. Effects of formalin fixation

on magnetic resonance indices in multiple sclerosis cortical gray matter. J Magn Reson Imaging. 2010;32(5):1054–1060.

40. Schmierer K, Tozer DJ, Scaravilli F, et al. Quantitative magnetization transfer imaging in postmortem multiple sclerosis brain. J Magn Reson Imaging. 2007;26(1):41–51.

41. Filippi M, Preziosa P, Rocca MA. Microstructural MR Imaging Techniques in Multiple Sclerosis. Neuroimaging Clin N Am. 2017;27(2):313–333.

42. Abdel-Fahim R, Mistry N, Mougin O, et al. Improved detection of focal cortical lesions using 7 T magnetisation transfer imaging in patients with multiple sclerosis. Mult Scler Relat Disord. 2014;3(2):258–265.

43. Seidal T, Balaton A, Battifora H. Interpretation and Quantification of Immunostains. Am J Surg Pathol. 2001;25(9):1204–1207.

44. Becker RJ. Standardization and Quality Control of Quantitative Microscopy in Pathology. J Cell Biochem Suppl. 1993;17G:199–204.

45. Walker R. Quantification of Immunohistochemistry--Issues Concerning Methods, Utility and Semiquantitative Assessment I. Histopathology. 2006;49(4):406–410.

46. Gilmore CP, Geurts JJG, Evangelou N, et al. Spinal cord grey matter lesions in multiple sclerosis detected by post-mortem high field MR imaging. Mult Scler. 2009;15(2):180–188.

47. Dolezal O, Dwyer MG, Horakova D, et al. Detection of Cortical Lesions is Dependent on Choice of Slice Thickness in Patients with Multiple Sclerosis. Int Rev Neurobiol. 2007;79(07):475–489.

48. Geurts JJG, Bö L, Pouwels PJW, Castelijns JA, Polman CH, Barkhof F. Cortical lesions in multiple sclerosis: Combined postmortem MR imaging and histopathology. Am J Neuroradiol. 2005;26(3):572–577.

49. Seewann A, Vrenken H, Kooi EJ, et al. Imaging the tip of the iceberg: Visualization of cortical lesions in multiple sclerosis. Mult Scler J. 2011;17(10):1202–1210.

50. Maranzano J, Dadar M, Rudko DA, et al. Comparison of multiple sclerosis cortical lesion types detected by multicontrast 3T and 7T MRI. Am J Neuroradiol. 2019;40(7):1162–1169.

Figure 1. MTR acquisition and immunohistochemistry.

MTR acquisition of a fixed brain slice is shown (**a**), with a leukocortical lesion, as demarcated by the dotted line on high magnification MTR (**b**) and corresponding myelin immunostaining (SMI94; in **c** scale bar is 500µm). Detailed pathology is presented (**d-f**), with myelin loss (SMI94; in **d** scale bar is 100µm), infiltrates of macrophages (CD68; in **e** scale bar is 100µm) and astrocytes (GFAP; in **f** scale bar is 100µm).

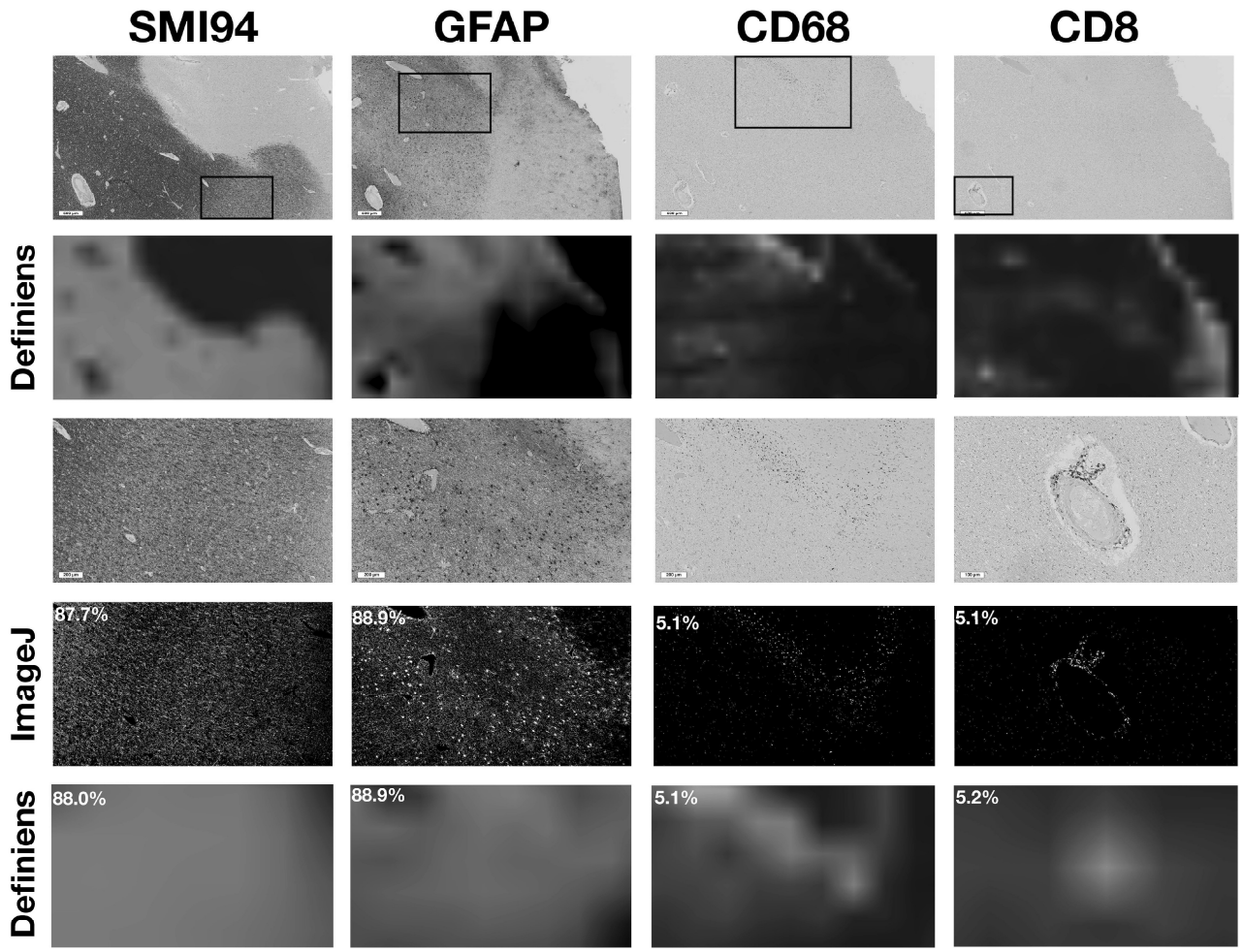

Figure 2. Image processing, quantification and data extraction.

Figure shows images of representative immunostains (SMI94, GFAP, CD68, CD8) (500 µm scale bar), and corresponding digitized images, obtained with Definiens Tissue Studio 3.6. For the purposes of this figure, we selected high magnification tissue sections (200 µm scale bar for SMI94, GFAP and CD68, and 100 µm scale bar for CD8) with a leukocortical lesion with activation of astrocytes and macrophages and perivascular infiltrates of CD8 lymphocytes. Area fraction obtained with ImageJ (version 1.5.2) and immunostain intensity obtained on 3D Slicer (version 4.4.0) are presented.

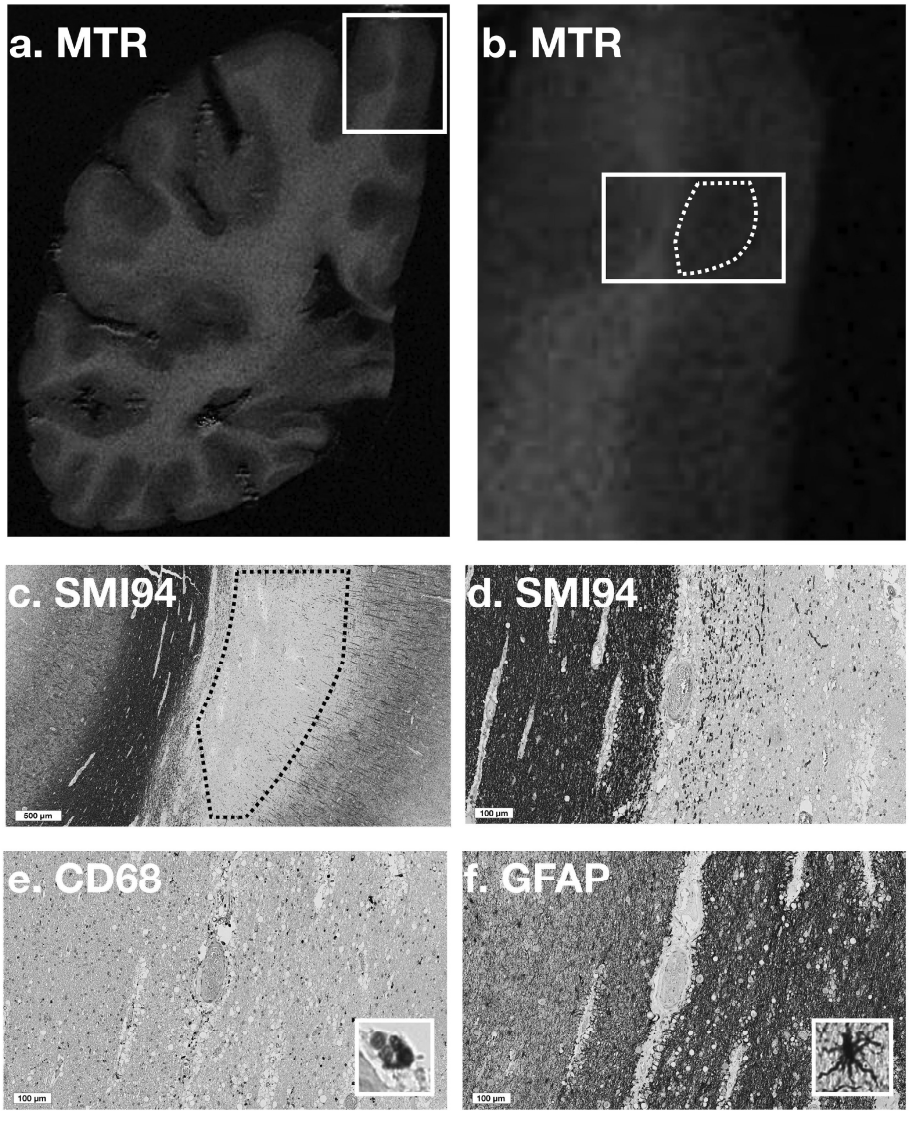

Figure 3. MTR values across ROIs in MS brains.

Box-and-Whisker plots show mean MTR values across ROIs in MS brains. WM lesions showed lower MTR than NAWM, and cortical GM lesions showed lower MTR than cortical NAGM; additionally, lower MTR was seen in the cortical NAGM than NAWM.

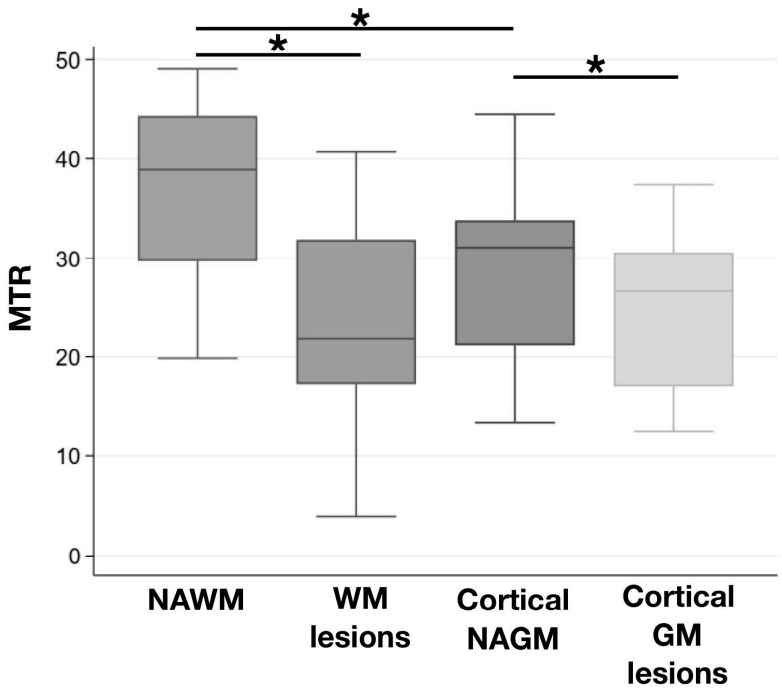

Figure 4. Associations between MTR and immunostaining intensities.

Scatter plots show associations between mean MTR values (y-axis) and mean immunostaining intensity (x-axis) for SMI94 (myelin) (**a**), CD68 (macrophages) (**b**), GFAP (astrocytes) (**c**), and mitochondrial damage (**d**), for each region-of-interest (NAWM in red, WM lesions in blue, cortical NAGM in green, and cortical GM lesions in yellow). Coefficients (Coeff) and 95% confidence intervals (95%CI) are shown from linear mixed-effects regression models accounting for the hierarchical structure of data (cassettes nested within patients).

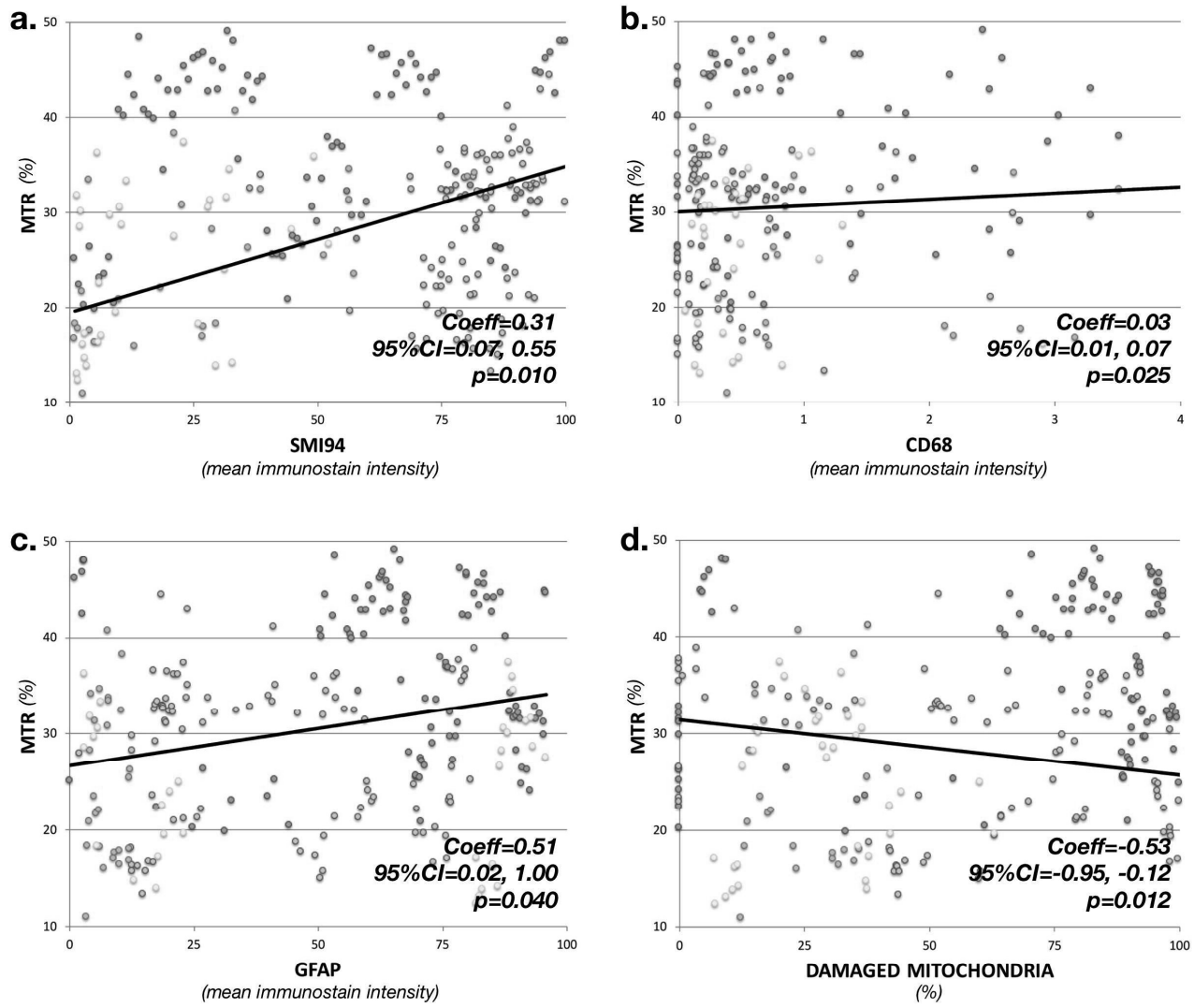

Table 1. Parameters for MRI acquisition.

	Echo Time *(ms)*	Relaxation time *(ms)*	Resolution *(mm)*	Field of View *(mm)*	Scan time *(minutes)*
PD/T2	12/80	4000	0.25×0.25×2.00	160×160×16	85
3D-T1	6.9	15	0.50×0.50×0.50	160×160×60	75
MTR	5.5/12.7	37	0.25×0.25×2.00	160×160×60	47

MRI: magnetic resonance imaging; PD: proton density-weighted sequence; T2: T2-weighted sequence; 3D-T1: T1-weighted sequence; MTR: magnetization transfer ratio.

Table 2. Characteristics of MS cases and healthy controls.

	MS *(n=16)*	***Controls*** *(n=4)*
Age, *years*	66.1±7.1	72.5±7.8
Gender, *female (%)*	10 (62.5%)	2 (50.0%)
Death-to-fixation interval, *hours*	28.8±11.6	20.2±10.5
Cassettes, *number from each slice*	5.2±1.0	4.5±0.6

Table 3. Associations between MTR values and immunostaining intensities.

	NF200				SMI94				CD68				CD20			
	Coeff	*95%CI*		*p-value*	*Coeff*	*95%CI*		*p-value*	*Coeff*	*95%CI*		*p-value*	*Coeff*	*95%CI*		*p-value*
1. Univariate models in MS brains																
	-0.01	-0.44	0.40		0.31	0.07	0.55		0.03	0.01	0.07		-0.01	-0.02	0.01	
2. Interaction term between ROIs in MS brains																
NAWM	*Reference*				*Reference*				*Reference*				*Reference*			
WM lesion	0.38	-0.31	1.09		1.58	1.09	2.08		0.16	0.09	0.22		-0.01	-0.03	0.02	
Cortical NAGM	0.51	-0.01	1.04		0.17	-0.21	0.56		-0.01	-0.06	0.04		0.01	-0.01	0.03	
Cortical GM lesion	0.37	-0.38	1.12		0.66	0.13	1.20		-0.04	-0.12	0.02		0.01	-0.02	0.03	
3. Interaction term between MS brains and controls																
	0.55	-0.60	1.70		-0.02	-0.84	0.79		1.40	0.56	2.25		0.01	-0.01	0.04	
4. Multivariate model in MS brains																
	-0.25	-0.57	0.05	*0.110*	0.31	0.09	0.52	*0.004*	0.01	-0.01	0.04	*0.203*	-0.01	-0.02	0.00	*0.147*

CD3				CD8				GFAP				IBA1				Mitochondrial damage			
Coeff	*95%CI*		*p-value*	*Coeff*	*95%CI*		*p-value*	*Coeff*	*95%CI*		*p-value*	*Coeff*	*95%CI*		*p-value*	*Coeff*	*95%CI*		*p-value*
-0.01	-0.02	0.01		-0.01	-0.04	0.01		0.51	0.02	1.00		0.13	-0.15	0.42		-0.53	-0.95	-0.12	

Reference				*Reference*				*Reference*				*Reference*				*Reference*			
0.01	-0.01	0.03		-0.02	-0.05	0.01		-0.43	-1.34	0.46		0.30	-0.11	0.72		0.22	-0.73	1.18	
0.01	-0.01	0.02		-0.01	-0.03	0.02		-0.64	-1.32	0.03		-0.37	-0.68	0.05		-1.07	-1.83	-0.31	
0.01	-0.01	0.04		-0.02	-0.07	0.02		-1.41	-2.30	-0.52		-0.33	-0.78	0.11		-0.65	-1.73	0.43	
0.01	-0.01	0.05		-0.01	-0.07	0.03		2.66	1.31	4.01		0.41	-0.29	1.12		-12.59	-23.16	-2.02	
-0.01	-0.01	0.01	*0.301*	-0.01	-0.03	0.01	*0.357*	-0.01	-0.35	0.34	*0.995*	0.05	-0.26	0.37	*0.728*	-1.34	-2.81	0.12	*0.074*

Table shows results of linear mixed-effects regression models accounting for the hierarchical structure of data (cassettes nested within patients), and evaluating associations between MTR and different immunostaining intensities in MS brains (**1**), differences in these associations between ROIs (interaction term between MTR and ROI, using NAWM as reference) (**2**), and differences in these associations between MS brains and controls (interaction term between MTR and case/control status, using controls as reference) (**3**). The final row shows the results from the multivariate model using a generalized structural equation modelling and including all immunostains (primary analysis) (**4**). Results are shown as Coeff, 95%CI and p-values.

MTR: magnetization transfer ratio; MS: multiple sclerosis; ROI: region of interest; Coeff: coefficient; 95%CI: 95% confidence interval; NA: normal appearing; WM: white matter; GM: grey matter.